Coherent Diffraction Imaging with Partially Coherent Discharge Plasma based EUV Sources

Jan Bußmann[1,2], Michal Odstrcil[2,3], Raoul Bresenitz[1,2], Mikheil Mebonia[2], Yusuke Teramoto[4], Marco Perske[5], Torsten Feigl[5], William S. Brocklesby[3] and **Larissa Juschkin**[1,2]

[1] Experimental Physics of EUV, JARA-FIT, RWTH Aachen University, Steinbachstraße 15, 52074 Aachen, Germany
[2] Peter Grünberg Institut (PGI-9), JARA-FIT, Forschungszentrum Jülich GmbH, 52425 Jülich, Germany
[3] Optical Research Centre, University of Southampton, Southampton, SO17 1BJ, UK
[4] BLV Licht- und Vakuumtechnik GmbH, Steinbachstrasse 15, 52074 Aachen, Germany
[5] OptiXfab GmbH, Hans-Knoell-Str. 6, 07745 Jena, Germany

Coherent Imaging with Extreme Ultraviolet Light

- Coherent diffraction imaging utilizes coherent light for lens-less imaging
- The intensity of the diffraction pattern of the object is recorded
- Iterative phase retrieval algorithm reconstructs phase and amplitude of the wavefront behind the object[3]
- Spatially resolved information about refractive index, material and thickness can be extracted
- Resolution does not directly depend on optics quality
- Ptychography (Scanning CDI) collects multiple patterns with overlapping illumination

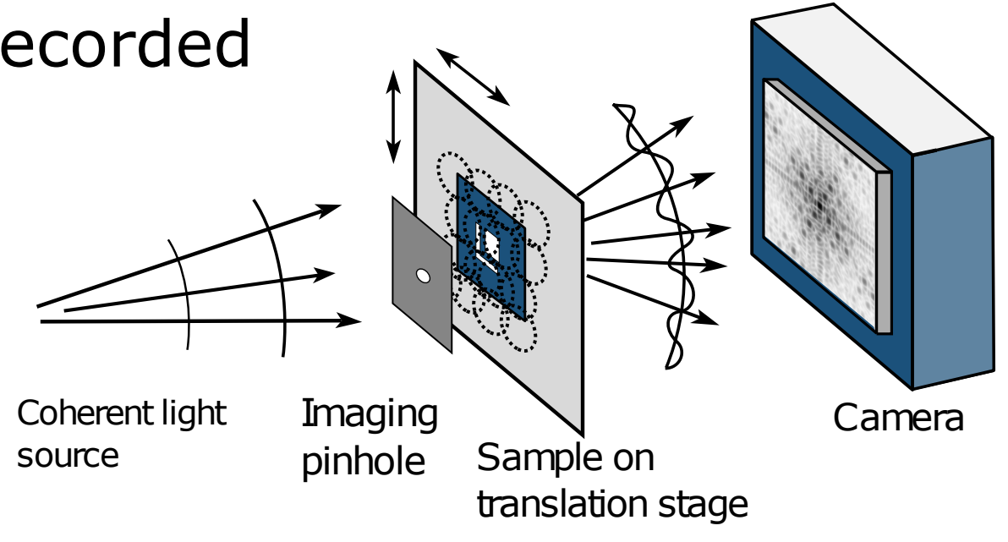

Schematic of a Ptychography Setup

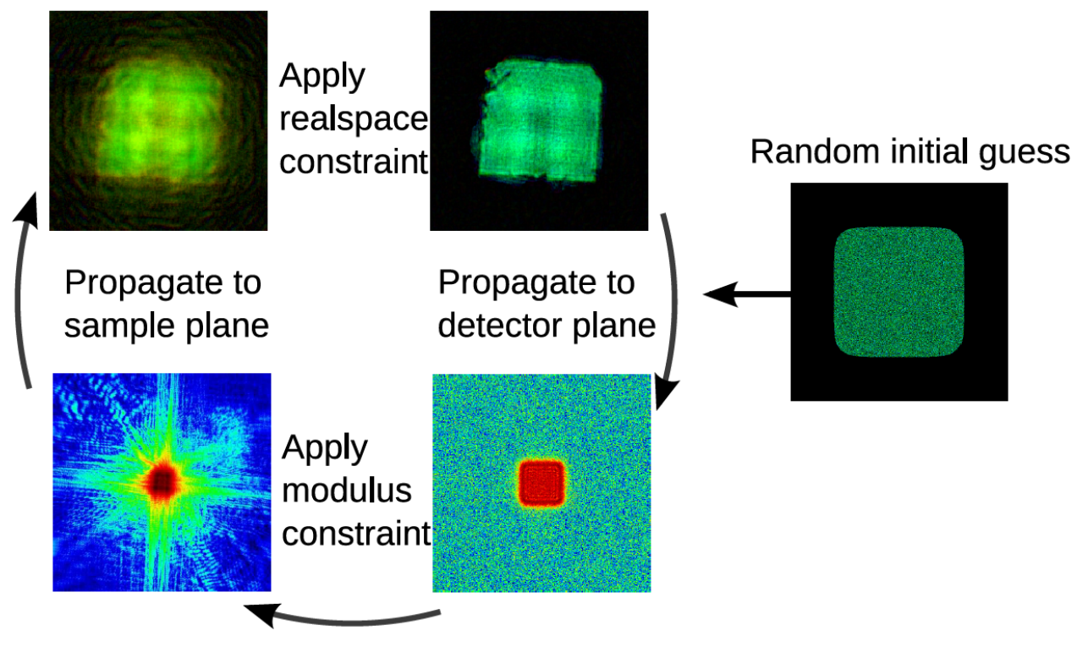

CDI	vs.	Ptychography
✔ "Single" image reconstruction		✔ "Infinite" sample size
✔ Highest resolution		✔ Robust reconstruction
		✔ Reconstruction of experimental conditions
✘ Fragile reconstruction		✘ Multiple images required
✘ Finit sample size		✘ Higher complexity

Top: Typical procedure for CDI reconstruction. Different constraints are applied to recover the wavefront at sample plane.

Right: The schematic shows how the algorithm slowly converges to a - in this case - optimal and unique solution.

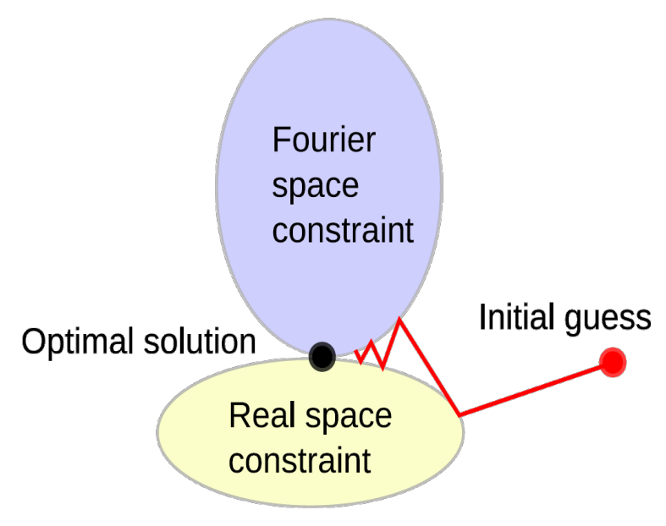

Gas Discharge Plasma EUV Light Sources

- Gas discharge at high voltages (2-3 kV) and 1-10 J p.P.
- Compression and heating lead to multiply ionized atoms (i.e. O^{5+}, Xe^{10+})
- Gas species, pressure and voltage determine emission spectrum and EUV output power

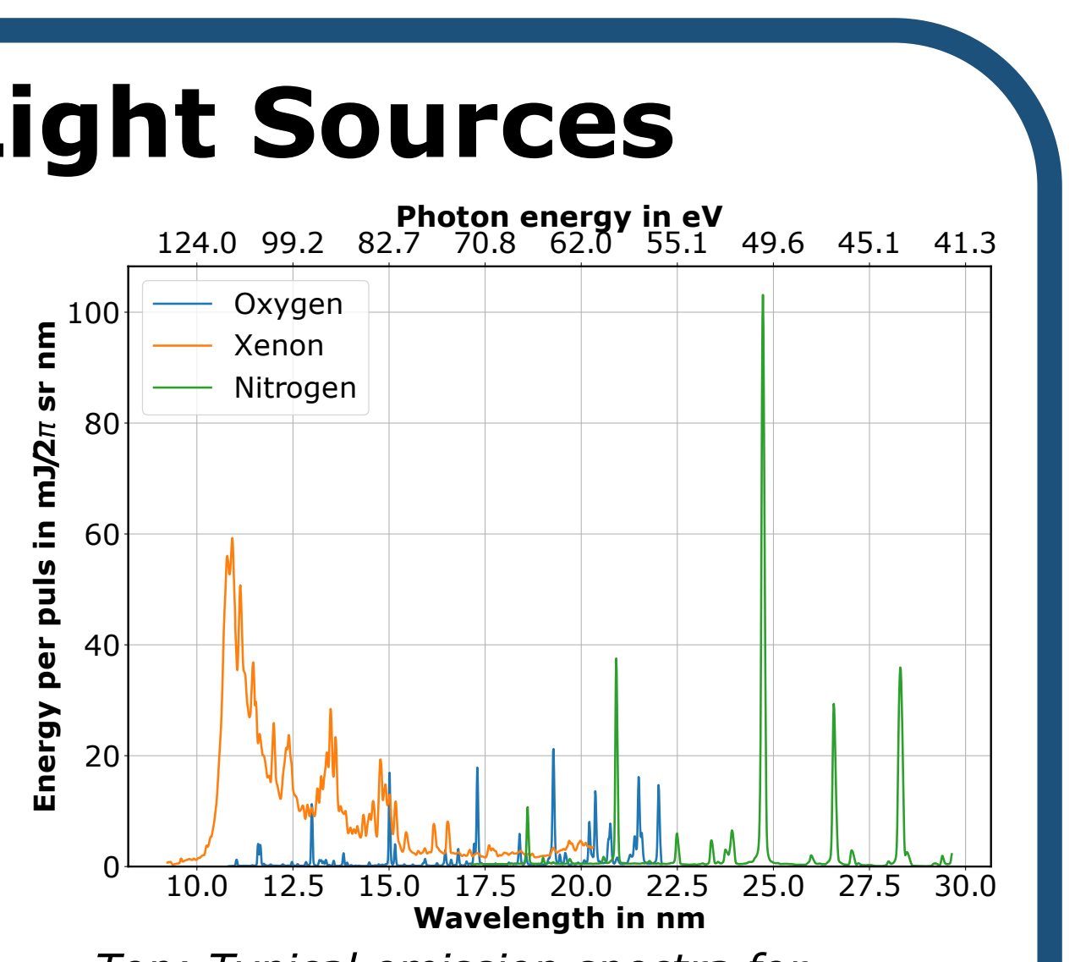

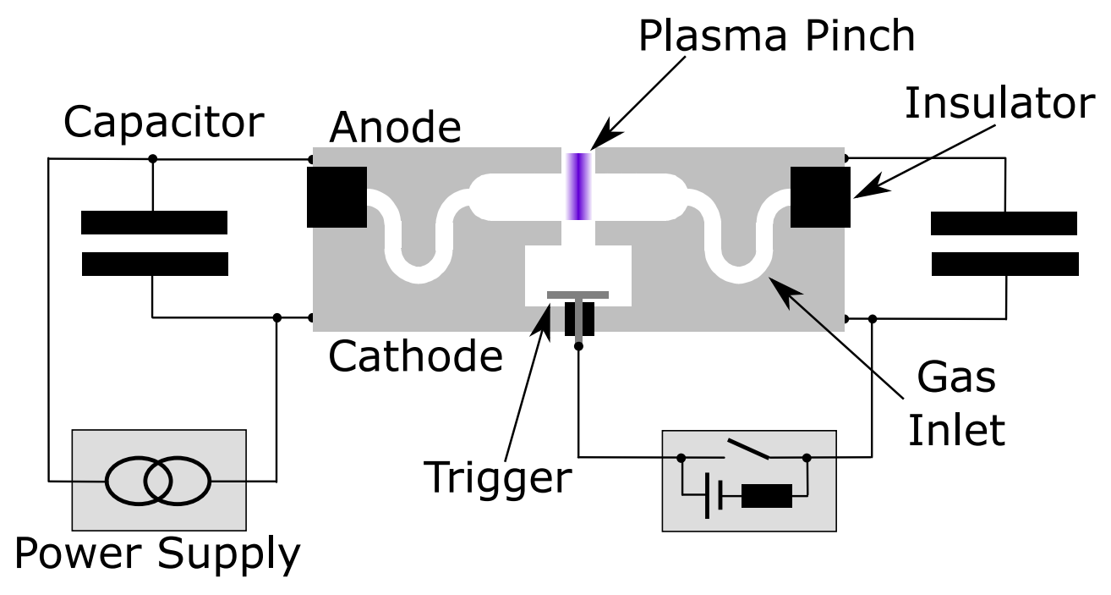

Top: Typical emission spectra for different gases. The resolution is mostly limited by the instrument function.
Middle: Schematic of a hollow-cathode triggered source based on [14]. The electrode material is molybdenium.
Left: Photography of a EUV source with its control electronics and cooling.

Features

- Emission of soft X-rays and EUV radiation (2 nm - 50 nm)
- High Power: 40 W/(2πsr) (@13.5 nm, 2% BW)
- Radiance from different emission lines:
  - 100 W/(mm^2 sr) (@10.9 nm, Xe/Ar, 4% BW)
  - 8 W/(mm^2 sr) (@13.5 nm, Xe, 3.2% BW)
  - 0.4 W/(mm^2 sr) (@17.3 nm, O_2, <0.1 % BW)

Applications

- Lithography[7]
- Mask defect inspection[8,9,10]
- Reflectometry[6]
- Scatterometry[5]
- Magneto-optical spectroscopy[4]
- Photoelectron spectro-microscopy[13]

Coherent Imaging in Farfield Regime

- Simple setup
- High dynamic range recording required, to detect high spatial frequency signals at the edge of the detector

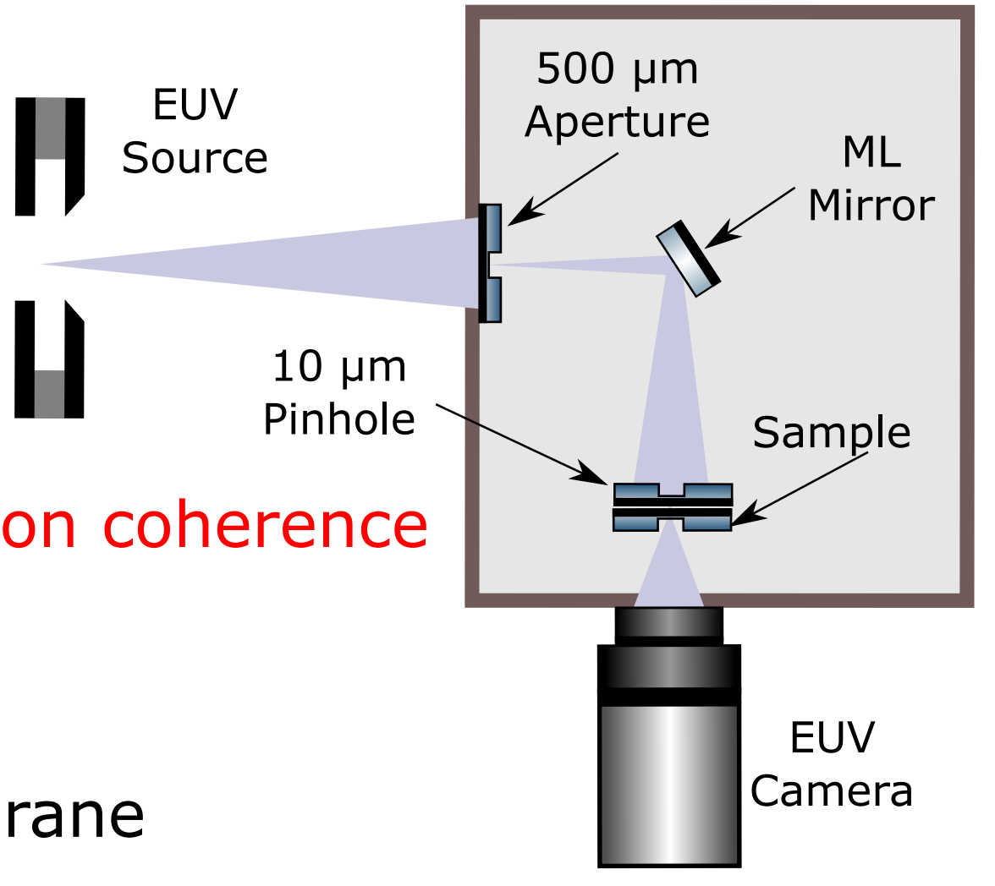

Imaging setup with a ML mirror and aperture for beam shaping. Sample and camera are separted by 4 cm.

Farfield Advantages	*Farfield Disadvantages*
✔ Highest achievable resolution	✘ Highest requirement on coherence
✔ Robust against vibrations	✘ Small Field of View

Experiment[1,2,11,12]

- Imaging (@17.3 nm) of a pattern in an Au/ Si_3N_4 membrane
- Reconstruction with a modified Hybrid-Input-Output algorithm and a modified modulus constraint[17,18]
- Three different Si_3N_4 thicknesses are distinguishable
- Resolution estimated to be 108 nm by PRTF [10] and 123 nm by knife-edge
- Inhomogenoues milling of FIB visible in the fan of the structure

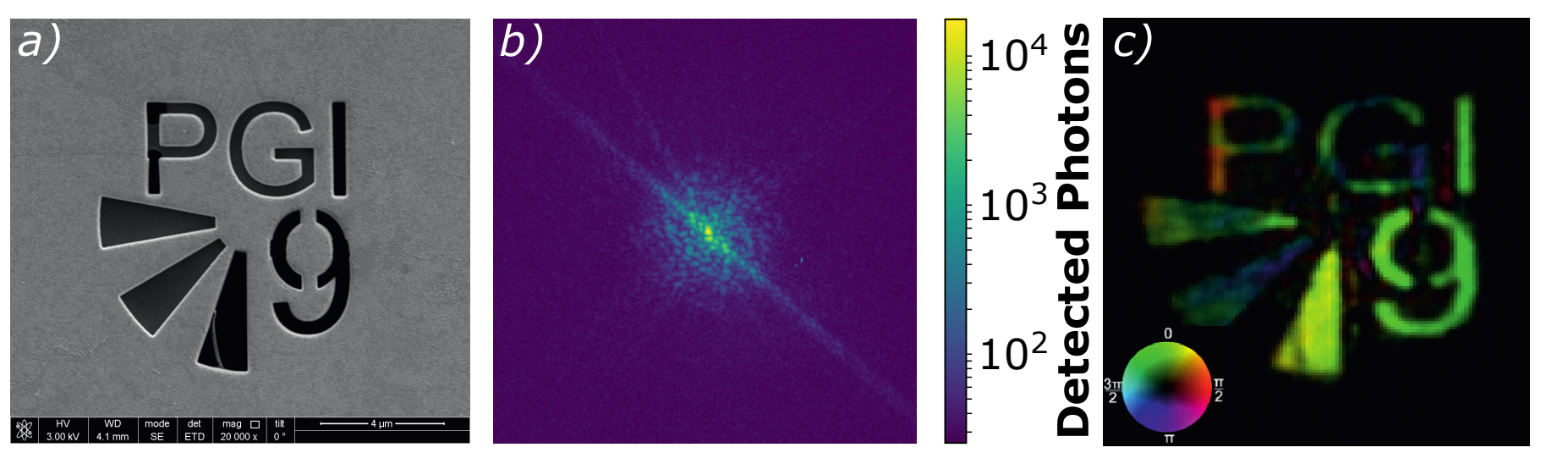

Top: a) Shows a SEM image of FIB-milled structure with different milling depths. Overall diameter is 9 µm. b) shows the diffraction pattern on the detector. c) The reconstructed objetc with the color-coded phase and amplitude.

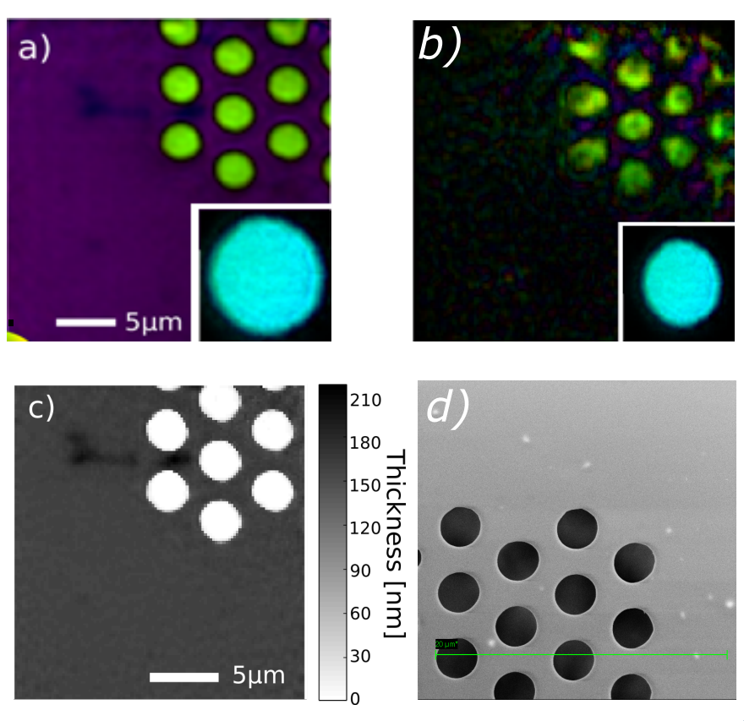

Right: a) Shows the reconstruction of a holey SiN-grid at 17.3 nm. b) Shows the reconstruction using the extracted 18.5 nm illumination from the same data set. c) shows the calcualted thickness map. d) is a SEM image of the grid.

Coherent Imaging in Nearfield Regime

- Nearfield regime F ~ 1 relaxes the requirement for high dynamic range imaging
- Fresnel scaling allows increased sample-detector distance
- Diffuser scatters light back to detector, which would not have reached it elsewise [15]

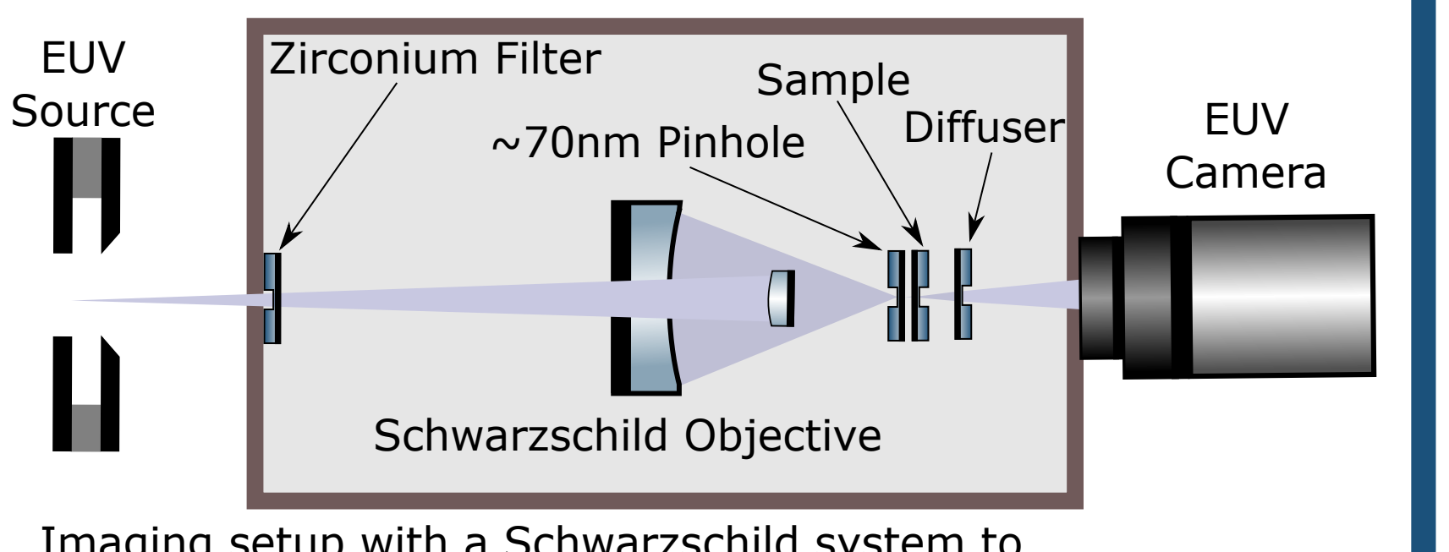

Imaging setup with a Schwarzschild system to demagnify the source onto a pinhole. Sample and pinhole separation is about 100 µm.

Nearfield Advantages	*Nearfield Disadvantages*
✔ Adjustable Field of View	✘ More complex setup
✔ Imaging of weak scatterer	✘ Strongly depending on pinhole size and distances
✔ Reduced requirements on coherence	

Experiment

- Strong curvature R=100 mm of an EUV-Schwarzschild objective gives access to the nearfield regime by Fresnel scaling
- Reconstruction of illumination wavefront even without visible diffraction speckles in the diffraction pattern
- By switching to a 70 nm pinhole a resolution of about 70 nm can be expected

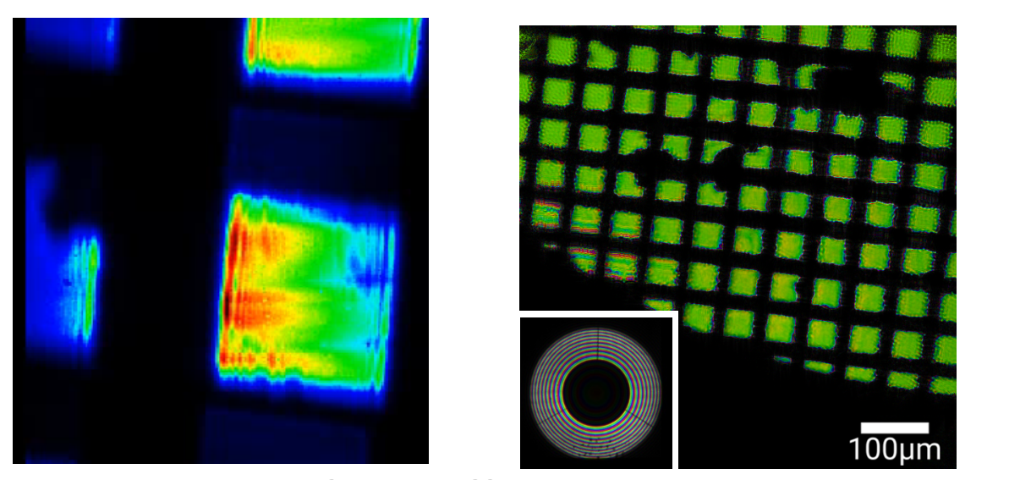

Left: Shows a nearfield diffraction pattern by a ~ 1 µm pinhole with visible fringes in one direction.
Coherence in the other direction was surpressed by another close-by pinhole.
Right: Reconstructed image of a nearfield pattern with a ~ 5 µm pinhole. Reconstruction artefacts due to bending of the sample and incoherence of the source.
Inset: Reconstructed illumination wavefront.

Farfield Ptychography with an Industrial Tin Plasma Source

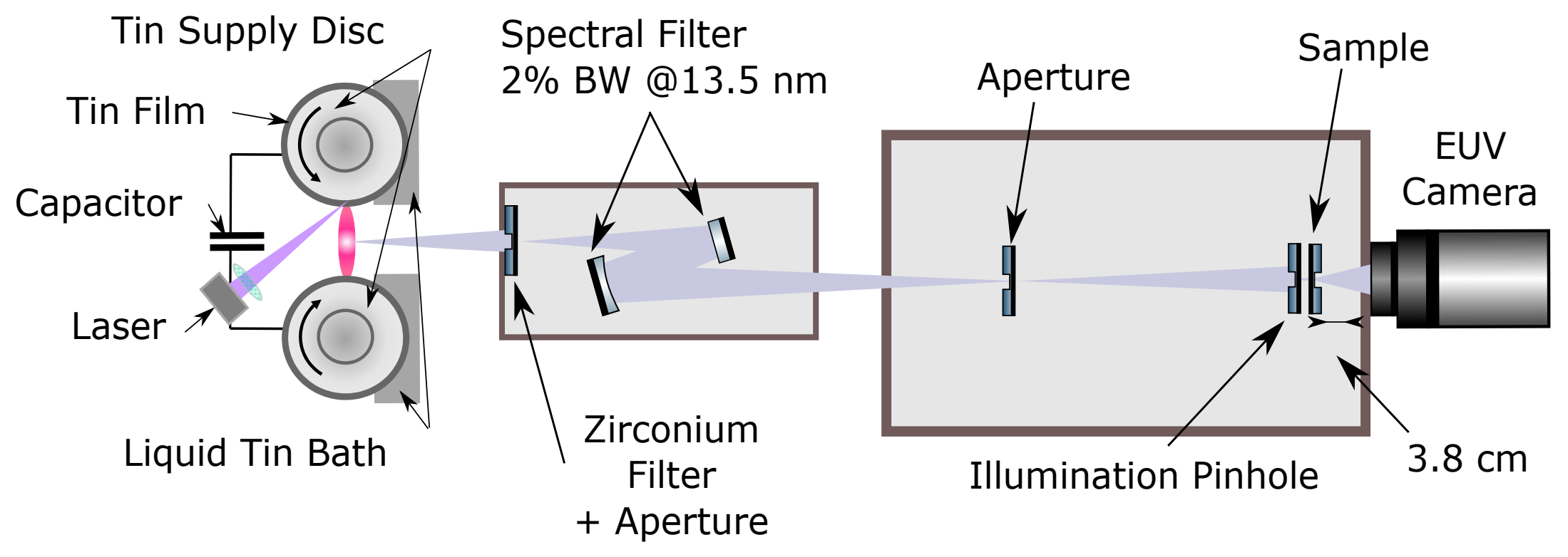

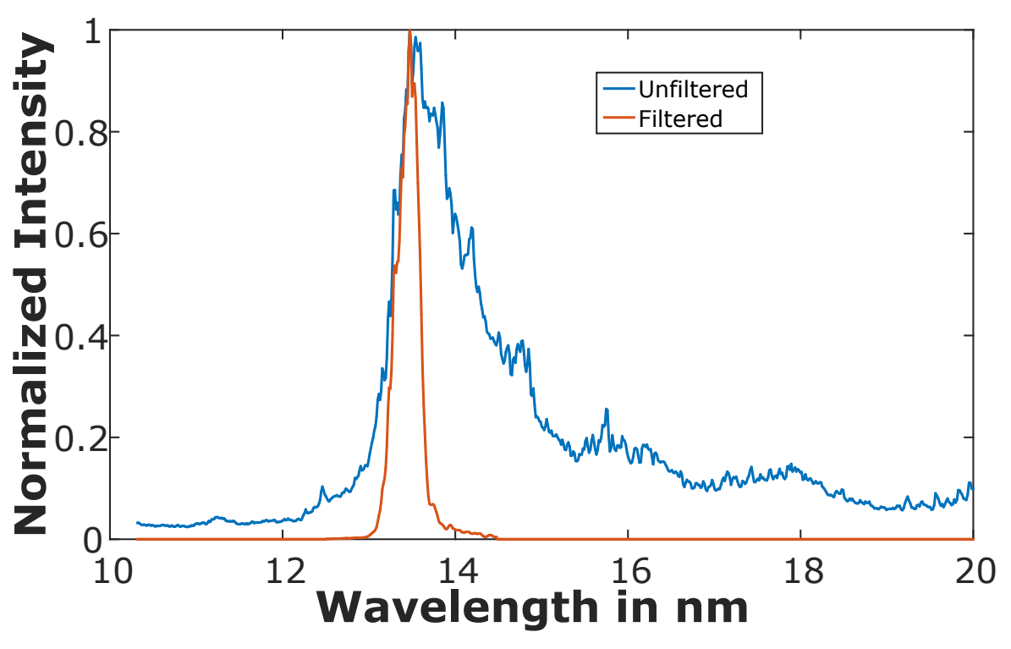

In blue the emission spectrum of the tin discharge source with a strong UTA at 13.5 nm. The orange line shows the light after passing the spectral filter.

- Industrial EUV metrology source
- Up to 300 W/(2πsr) and 145 W/(sr mm^2) (2% BW)

Experiment

- 200 scanning positions ea 30 s exposure
- 400 nm polyspheres show strong phase contrast
- Thickness determination in principle possible, but limited by resolution
- 100 nm resolution for ~ 50 µm FoV
- Application for pellicle inspection
- Further information in [19]

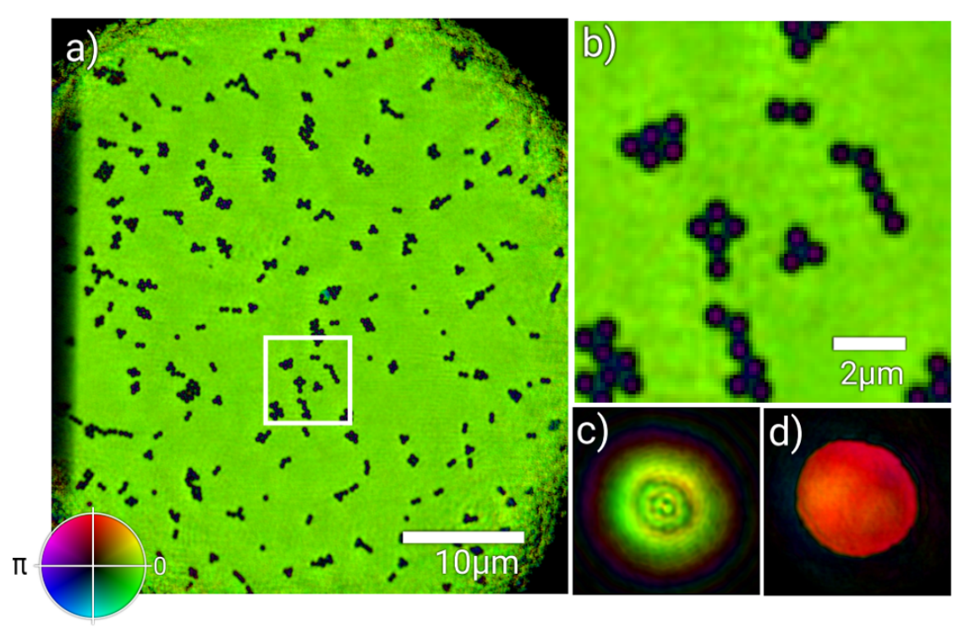

Figure a) Reconstructed image. Figure b) shows a zoomed version, with a significant phase shift visible. c) shows the illumination wavefront on the sample, d) shows the backprojection to the pinhole position.

Acknowledgment to: USHIO

Outlook: Actinic Inspection of Defects in Multilayer Mirrors by Reflection Ptychography

- Particles/ defects on mask blanks are one of the major challenge in EUV lithography/ imaging
- Development of deposition technique to cover these defects
- Fabrication of programmed defects arrays with different defect sizes
- Inspection of defects by non actinic methods (AFM, SEM,..) is limited in validity
- EUV light can penetrate the multilayers to probe the influence of the defects

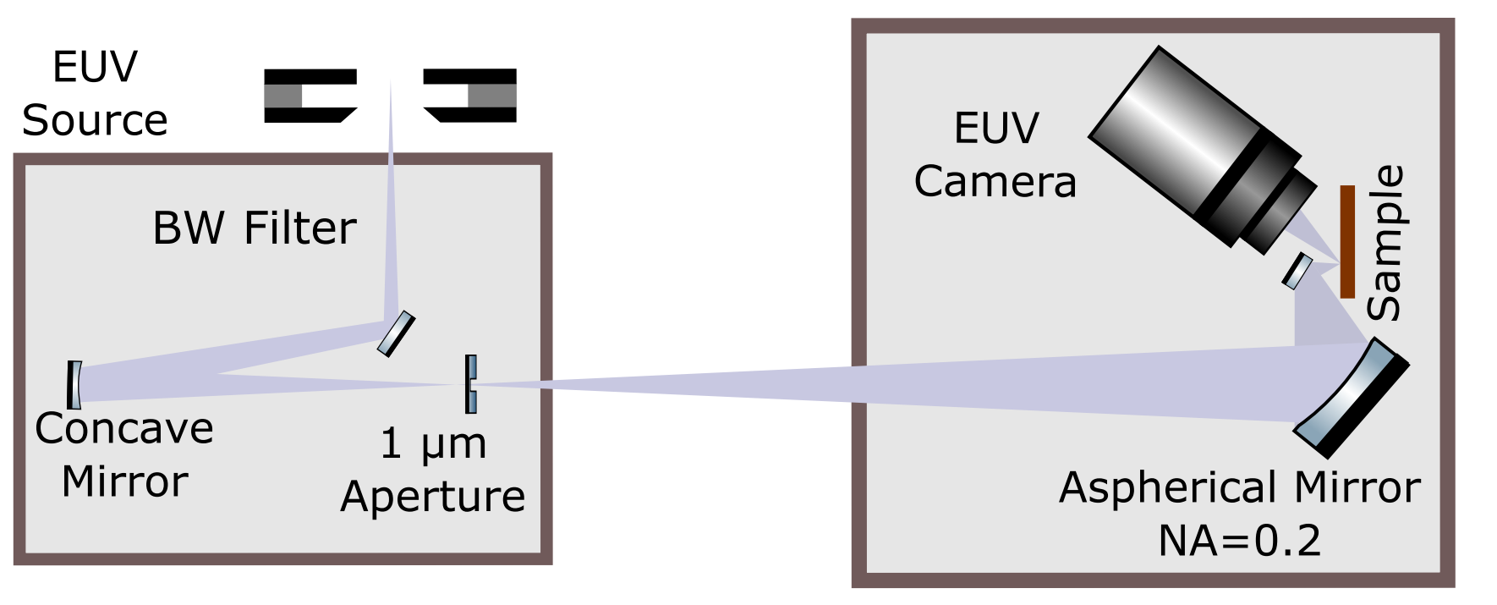

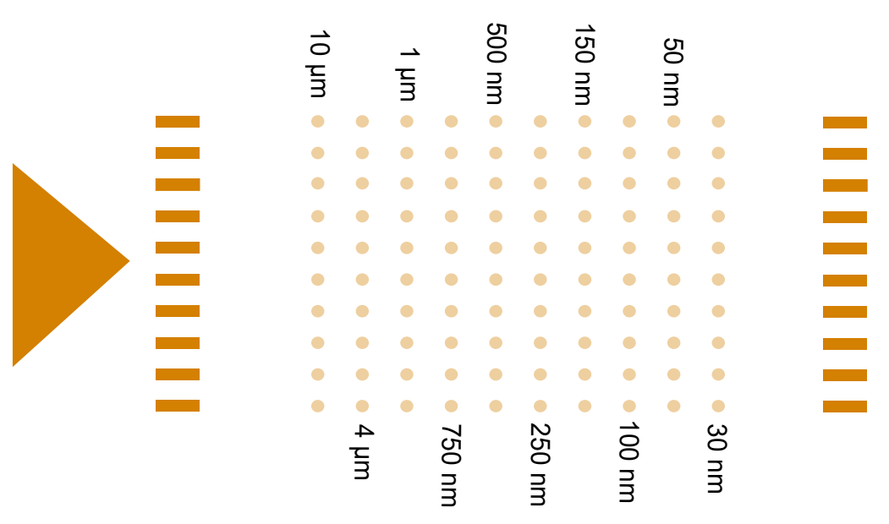

Drawing of the defect array with labeld dot sizes.

Experiment

- Fully coherent illumination of a 8 cm aspherical mirror to create a coherent spot of 10 - 50 µm on the multilayer sample
- Dual mirror setup allows flexible adjustment of bandwidth of 2% and smaller with a peak reflectivity of 13% (@13.5 nm)
- 1 µm pinhole at source image position allows adjustment of spatial coherence

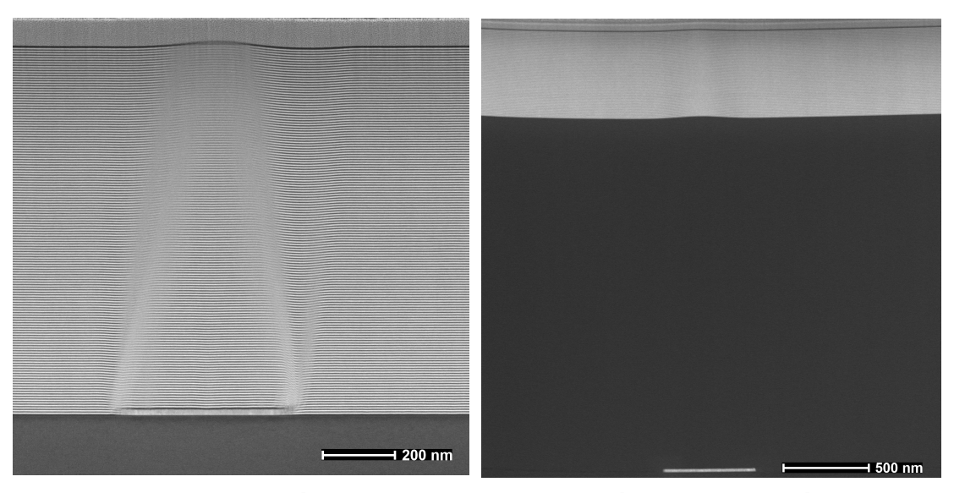

TEM Micrographs of a 500 nm diameter defect buried below 144 ML of Si/Mo (left) and an additional 2 µm Si smoothing layer (right).

Project Partner: optiX fab.

Founding: ZIM Zentrales Innovationsprogramm Mittelstand

[1] L. Juschkin et al., Proc. SPIE, 88490 (2013)
[2] J. Bußmann et al., Springer Proceedings, X-Ray Lasers 2014 (2016)
[3] J.R. Fienup, Apl. Opt. 21, 2758 (1982)
[4] D. Wilson et al., Rev. Sci. Instrum. 85, 103110 (2014)
[5] M. Wurm et al., DGaO-Proceedings (2006)
[6] S. Danylyuk et al., Phys. Stat. Sol. C 12, 318-322 (2015)
[7] S. Danylyuk et al., Vac. Sci. Technol. B 31, 021602 (2013)
[8] A. Maryasov et al., Proc. SPIE, 7985 (2011)
[9] L. Juschkin et al., J. Phys. Conf. Ser. 186, 012030 (2009)
[10] H. N. Chapman et al., J. Opt. Soc. Am A. 5, 1179 (2006)
[11] L. Juschkin et al., Proc. SPIE, 8678 (2012)
[12] J. Bußmann et al., Proc. SPIE, 9589 (2015)
[13] M. Odstrcil et al., Opt. Lett. 40, 23 (2015)
[14] C. Schmitz et al., Appl. Phys. Lett. 23, 108 (2016)
[15] M. Benk, Thesis, RWTH Aachen University (2011)
[16] M. Stockmar et al., Scientific Reports, 3 (2013)
[17] B. Zhang et al., Proc. SPIE, 9050 (2014)
[18] S. Marchesini et al. , PRB 68, 140101 (2003)
[19] J. Bußmann et al., JARA-FIT Report 2015, (2016)

Poster Download

Business Card

larissa.juschkin@rwth-aachen.de